*Int. J. Heat Mass Transfer.* Vol. 34, No. 10, pp. 2535–2543, 1991
Printed in Great Britain

0017–9310/91 $3.00 + 0.00


# Dynamic responses in hollow concrete cylinders under hazardous thermal loads

C. L. D. HUANG and GAMAL N. AHMED
Department of Mechanical Engineering, Kansas State University, Manhattan, KS 66506, U.S.A.

(*Received* 6 *July* 1990 *and in final form* 26 *November* 1990)

**Abstract**—Prediction of the structural integrity of high temperature nuclear reactors under hostile thermal environments is of considerable concern in safety assessments of reactors. A mathematical model, simulating the coupled heat and mass transfer in concrete structures exposed to extremely high temperatures, has been developed and numerically solved. With the prediction of the pore pressure, temperature, and moisture redistribution, the effect of various rates of thermal loads on the concrete response is investigated. The rate of moisture clog penetration into the concrete cylinder and hence the locations of the maximum pore pressure peaks developed under different rates of the severe thermal loads are determined. Thus, the possibilities of concrete spallings occurring under these conditions are studied and predicted.

## INTRODUCTION

IN THE nuclear industry, concrete is heavily used as a structural material and forms a principal component of radiation shielding. Structural concrete used in high temperature reactors is exposed to high thermal and mechanical stresses during the reactor's working and/or accidental conditions. As a result, the induced gradients of temperature and pore pressure in concrete provoke internal stresses which may cause microcracks and explosive spallings of concrete. Under such severe environmental conditions, the integrity of concrete is questionable; and hence, the prediction of the effect of coupled heat and mass transfer in concrete becomes important in safety assessments of nuclear reactors.

Numerous studies investigated the moisture transport in porous media induced by pore pressure gradients. The hygrothermal behavior of concrete slabs under normal ambient conditions was reported in refs. [1–5]. England and Sharp [6], and Dhatt *et al.* [7] investigated the safety of nuclear reactors and the behavior of materials under the effect of high temperatures.

In recent years, engineering analyses on concrete structures subjected to elevated temperatures were performed to investigate moisture transfer which was attributed to the evaporation–condensation mechanism driven by high pressure and moisture concentration gradients [8, 9]. Their results have been compared with experimental data. Bazant and Thonguthai [10] studied the coupled heat and mass transfer in concrete at high temperatures using the finite element method. Moisture losses obtained by calculation were compared with the measured data reported by Chapman and England [4]. Harmathy [11] and Schneider [12] reported a literature survey on the high temperature properties of concrete.

Concrete contains a fine porous system filled with adsorbable and evaporable water. Under the high temperature situation, convective and diffusive mass and heat transfer are involved simultaneously in concrete. These transport phenomena induce expansion and evaporation of gases, entrapped in the pores which generate high pressure and concentration gradients. As a result, the convective mass flow of gaseous mixture towards the heated and/or cold surfaces, driven by pore pressure gradient, is developed. This convective mass flow of gases is the dominant mechanism in the transport phenomena. Diffusive mass flow developed by the concentration gradient may enhance the evaporation rates as well. The pore pressure developed in porous concrete generates internal stresses which exceed the tensile strength of concrete and results in explosive spallings and cracks in the concrete.

Heat and mass transfer in concrete exposed to high temperatures or to high temperature gradients involve many physical interaction problems: (a) the pore pressure, temperature, and moisture content distributions are strongly coupled; (b) mass transfer involves multiphase (liquid and gaseous phases); and (c) the thermal and material parameters of porous media (such as permeability, conductivity, density, etc.) are highly non-linear functions of temperature, pressure, and moisture. Developing a mathematical model, capable of rationally determining structural response and correctly simulating the heat and mass transfer in concrete subjected to severe thermal loads, is a complex process. Nevertheless, predicting the response of concrete structures to extremely high temperatures is of considerable concern for safety assessments of nuclear reactors. An accurate but rather simple mathematical model is needed.

In this paper, the developed model is applied to study the dynamic responses of an axisymmetric hollow concrete cylindrical vessel exposed internally to several different hostile thermal environments. In par-

## NOMENCLATURE

$a_0$ reference permeability [m s$^{-1}$]
$C_p$ effective heat capacity [kJ kg$^{-1}$ K$^{-1}$]
$C_{pi}$ specific heat of the $i$th component at constant pressure [kJ kg$^{-1}$ K$^{-1}$]
$D$ modified diffusivity of gaseous mixture [m$^2$ s$^{-1}$]
$D'$ diffusivity of gaseous mixture [m$^2$ s$^{-1}$]
$e$ effective emissivity
$h_c$ convective heat transfer coefficient [W m$^{-2}$ K$^{-1}$]
$h_D$ mass transfer coefficient [kmol m$^{-2}$ K$^{-1}$]
$h_{es}$ heat transfer coefficient of the side exposed to high temperatures [W m$^{-2}$ K$^{-1}$]
$h_{us}$ heat transfer coefficient of the side exposed to atmospheric environment [W m$^{-2}$ K$^{-1}$]
$k$ effective thermal conductivity of the porous medium [W m$^{-1}$ K$^{-1}$]
$k_i$ thermal conductivity of the $i$th component of the porous medium [W m$^{-1}$ K$^{-1}$]
$k_g$ thermal conductivity of the gaseous mixture [W m$^{-1}$ K$^{-1}$]
$K_0$ Darcy's coefficient or coefficient of permeability [m$^3$ s kg$^{-1}$]
$m$ volumetric moisture content per unit volume of the porous system [m$^3$ m$^{-3}$]
$M$ molecular weight of the gaseous mixture [kg kmol$^{-1}$]
$M_i$ molecular weight of the $i$th component of the gaseous mixture [kg kmol$^{-1}$]
$P$ total pressure or pore pressure [N m$^{-2}$]
$Q$ latent heat of evaporation of free water [kJ kg$^{-1}$]
$R$ universal gas constant [kJ mol$^{-1}$ K$^{-1}$]
$t$ time [s]
$T$ absolute temperature [K]
$V_g$ bulk velocity of the gaseous mixture [m s$^{-1}$]
w/c free water–cement ratio [kg kg$^{-1}$]
$x$ space coordinate.

Greek symbols
$\Gamma$ mass rate of evaporation per unit volume of the porous system [kg m$^{-3}$ s$^{-1}$]
$\varepsilon$ porosity of the porous system
$\varepsilon_g$ volume fraction of the gaseous mixture [m$^3$ m$^{-3}$]
$\rho$ effective density of the porous system [kg m$^{-3}$]
$\rho_i$ mass of the $i$th component per unit volume of the $i$th component [kg m$^{-3}$]
$\sigma$ Stefan–Boltzmann constant [W m$^{-2}$ K$^{-4}$]
$\phi$ mole fraction of water vapor of the gaseous mixture [kmol kmol$^{-1}$].

Subscripts
a air in a gaseous mixture
atm atmosphere
d dry concrete
es at the exposed surfaces to fire
f fire
g gaseous mixture
$i$ $i$th component of the porous system
l liquid
s at the surface
us at the unexposed surfaces to fire
v vapor in a gaseous mixture
w water
0 initial condition or datum
$\infty$ ambient.

ticular, the changes in pore pressure, temperature, and moisture due to the variations of physical properties of a concrete vessel under the effect of high temperature are examined. The effects of various rates of thermal flux on a concrete vessel are examined.

## GOVERNING EQUATIONS

A mathematical model describing the coupled heat and mass transfer in porous media, such as concrete, is derived. The following assumptions concerning the porous system and the transport process are made: a multi-phase porous system is taken as a continuous medium; local thermodynamic equilibrium exists; a rigid solid matrix and incompressible liquid are assumed; mobility of liquid is assumed to be negligible as compared to that of gaseous mixture; water vapor, air, and their mixture are ideal gases; compressional work and viscous dissipation are negligible; and energy transferred by diffusion compared to conduction is negligible.

Given such assumptions and based on the concepts of continuum mechanics, such as principles of irreversible thermodynamics, conservation of mass, momenta, and energy, a set of three basic equations is derived as follows:

Conservation of mass for water liquid

$$\frac{\partial}{\partial t}\rho_w(\varepsilon-\varepsilon_g) = -\Gamma. \tag{1}$$

Conservation of mass for water vapor

$$\rho_v\varepsilon_g\frac{\partial\phi}{\partial t} - (1-\phi)\Gamma = -\rho_v\varepsilon_g V_g\cdot\nabla\phi + \frac{\rho_g}{\rho_a}\nabla\cdot(\rho_g\varepsilon_g D\nabla\phi) \tag{2}$$

where

$$D = M_w M_a D'/M^2 = D(\phi).$$

Conservation of mass for air component

$$-\rho_v \varepsilon_g \frac{\partial \phi}{\partial t} + (1-\phi)\Gamma = \rho_v \varepsilon_g V_g \cdot \nabla \phi - \frac{\rho_g}{\rho_a} \nabla \cdot (\rho_g \varepsilon_g D \nabla \phi). \quad (3)$$

Conservation of mass for the gaseous mixture

$$\frac{\partial}{\partial t}(\rho_g \varepsilon_g) + \nabla \cdot (\rho_g \varepsilon_g V_g) = \Gamma. \quad (4)$$

Conservation of energy equation

$$\rho C_p \frac{\partial T}{\partial t} + \rho_w Q \frac{\partial \varepsilon_g}{\partial t} = \nabla \cdot (k \nabla T) - \rho_g \varepsilon_g C_{p_g} V_g \cdot \nabla T. \quad (5)$$

The moisture content, $m$, is related to the pore pressure, $P$, temperature, $T$, and mole fraction of water vapor in the gaseous mixture, $\phi$, through a state equation, i.e. $m = m(P, T, \phi)$. This constitutive relation is given as a set of sorption isotherms for various temperatures of concrete through experimental techniques [8]. With the definition of the volume fraction of the gaseous mixture, $\varepsilon_g = \varepsilon - m(P, T, \phi)$, a set of three coupled non-linear second-order partial differential equations is obtained. For heat and mass transfer in an axisymmetric hollow concrete cylinder, this set of equations is given in the following form [13]:

$$A_k \frac{\partial \phi}{\partial t} + B_k \frac{\partial P}{\partial t} + C_k \frac{\partial T}{\partial t} = D_k \left[\frac{\partial^2 \phi}{\partial r^2} + \frac{1}{r}\frac{\partial \phi}{\partial r}\right] + E_k \left[\frac{\partial^2 P}{\partial r^2} + \frac{1}{r}\frac{\partial P}{\partial r}\right] + F_k \left[\frac{\partial^2 T}{\partial r^2} + \frac{1}{r}\frac{\partial T}{\partial r}\right] + G_k \left[\frac{\partial \phi}{\partial r}\right]^2 + H_k \left[\frac{\partial P}{\partial r}\right]^2 + I_k \left[\frac{\partial T}{\partial r}\right]^2 + J_k \left[\frac{\partial \phi}{\partial r}\frac{\partial P}{\partial r}\right] + K_k \left[\frac{\partial \phi}{\partial r}\frac{\partial T}{\partial r}\right] + L_k \left[\frac{\partial P}{\partial r}\frac{\partial T}{\partial r}\right] \quad (6)$$

where the coefficients $A_k, \ldots, L_k$ for $k = 1, 2, 3$ are functions of the dependent variables $\phi(r, t)$, $P(r, t)$, and $T(r, t)$. They are defined as follows:

$$A_1 = 1 - \left(\frac{(1-\phi)\rho_w}{(PM_w/RT)} \frac{1}{\varepsilon_g}\frac{\partial \varepsilon_g}{\partial \phi}\right)$$

$$A_2 = \left(1 - \frac{\rho_w}{PM/RT}\right)\frac{1}{\varepsilon_g}\frac{\partial \varepsilon_g}{\partial \phi} + \frac{M_w - M_a}{M}$$

$$B_1 = -\left(\frac{(1-\phi)\rho_w}{(PM_w/RT)} \frac{1}{\varepsilon_g}\frac{\partial \varepsilon_g}{\partial P}\right)$$

$$B_2 = \left(1 - \frac{\rho_w}{PM/RT}\right)\frac{1}{\varepsilon_g}\frac{\partial \varepsilon_g}{\partial P} + \frac{1}{P}$$

$$C_1 = -\left(\frac{(1-\phi)\rho_w}{(PM_w/RT)} \frac{1}{\varepsilon_g}\frac{\partial \varepsilon_g}{\partial T}\right)$$

$$C_2 = \left(1 - \frac{\rho_w}{PM/RT}\right)\frac{1}{\varepsilon_g}\frac{\partial \varepsilon_g}{\partial T} - \frac{1}{T}$$

$$D_1 = D', \quad D_2 = 0$$

$$E_1 = 0, \quad E_2 = K_D$$

$$F_1 = 0, \quad F_2 = 0$$

$$G_1 = D'\left(\frac{1}{\varepsilon_g}\frac{\partial \varepsilon_g}{\partial \phi} - \frac{M_w - M_a}{M}\right), \quad G_2 = 0$$

$$H_1 = 0, \quad H_2 = \frac{\partial K_D}{\partial P} + K_D\left(\frac{1}{\varepsilon_g}\frac{\partial \varepsilon_g}{\partial P} + \frac{1}{P}\right)$$

$$I_1 = 0, \quad I_2 = 0$$

$$J_1 = D'\left(\frac{1}{\varepsilon_g}\frac{\partial \varepsilon_g}{\partial P} + \frac{1}{P}\right) + K_D$$

$$J_2 = \frac{\partial K_D}{\partial \phi} + K_D\left(\frac{1}{\varepsilon_g}\frac{\partial \varepsilon_g}{\partial \phi} + \frac{M_w - M_a}{M}\right)$$

$$K_1 = D'\left(\frac{1}{\varepsilon_g}\frac{\partial \varepsilon_g}{\partial T} - \frac{1}{T}\right), \quad K_2 = 0$$

$$L_1 = 0, \quad L_2 = \frac{\partial K_D}{\partial T} + K_D\left(\frac{1}{\varepsilon_g}\frac{\partial \varepsilon_g}{\partial T} - \frac{1}{T}\right)$$

$$A_3 = \rho_w Q \frac{\partial \varepsilon_g}{\partial \phi}, \quad G_3 = 0$$

$$B_3 = \rho_w Q \frac{\partial \varepsilon_g}{\partial P}, \quad H_3 = 0$$

$$C_3 = \rho_w Q \frac{\partial \varepsilon_g}{\partial T} + \rho C_p, \quad I_3 = k' \frac{\partial \varepsilon_g}{\partial T}$$

$$D_3 = 0, \quad J_3 = 0$$

$$E_3 = 0, \quad K_3 = k' \frac{\partial \varepsilon_g}{\partial \phi}$$

$$F_3 = k(\varepsilon_g), \quad L_3 = k' \frac{\partial \varepsilon_g}{\partial P} + K_D(\rho_g \varepsilon_g C_{P_g})$$

$$M = \phi M_w + (1-\phi)M_a = M(\phi)$$

$$\rho C_p = (1-\varepsilon)\rho_s C_{p_s} + (\varepsilon - \varepsilon_g)\rho_w C_{p_w} + \rho_g \varepsilon_g C_{p_g}$$

$$k' = \frac{dk(\varepsilon_g)}{d\varepsilon_g}$$

$$k(\varepsilon_g) = [(1-\varepsilon)k_s^{1/4} + (\varepsilon - \varepsilon_g)k_L^{1/4} + \varepsilon k_g^{1/4}]^4.$$

## BOUNDARY CONDITIONS AND INITIAL CONDITIONS

Figure 1 shows a hollow concrete cylinder of inner radius $r_i = 80$ cm and outer radius $r_o = 100$ cm. The inner surface of the concrete cylinder is assumed to be exposed to various hostile environments in such a manner that the surface temperatures of the concrete

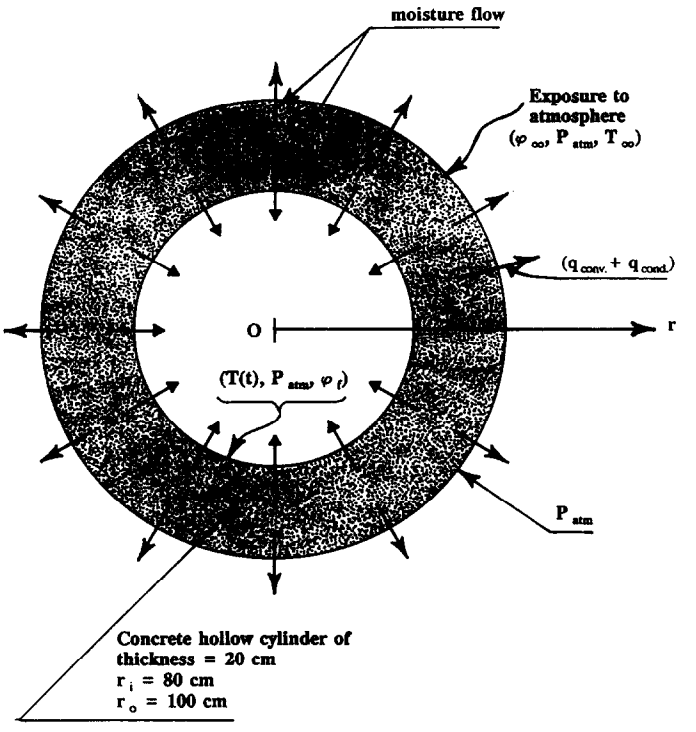


FIG. 1. Hollow concrete cylinder under the effect of various heating rates at the inner surface and surrounding atmosphere at the outer surface.

cylinder rise linearly at different rates. Representing different thermal effects of the various hypothetical accidents, the different temperature–time curves of the concrete surface are described in Fig. 2. At the outer surface of the concrete cylinder, heat and mass are transferred freely through the surface to the surrounding atmosphere. Therefore, the boundary conditions at the inner and outer surfaces of the simulated hollow concrete cylinder attacked by various hostile environments during the time duration of 7 h are:

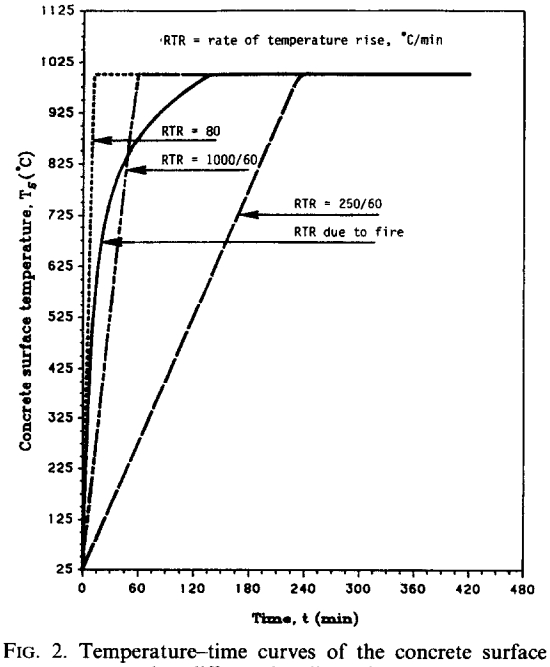


FIG. 2. Temperature–time curves of the concrete surface exposed to different hostile environments.

(1) $r = r_i$, inner surface

$$\phi = 0.0 \tag{7}$$

$$P = P_{atm} \tag{8}$$

(a) for inner surface exposed to fire

$$-k\frac{\partial T}{\partial r} = h_{es}[T_f(t) - T]$$

$$\text{for } T \leqslant 1000°C \quad \text{and } 0 \leqslant t \leqslant 7\,\text{h} \tag{9}$$

where

$$h_{es} = h_{c,es} + e\sigma[T_f(t) + T][T_f^2(t) + T^2];$$

(b) for inner surface exposed to other hostile environments

$$T_s(r_i, t) = \text{RTR} \cdot t,$$

$$\text{for } T_s \leqslant 1000°C \quad \text{and } 0 \leqslant t \leqslant 7\,\text{h} \tag{10}$$

where

$$\text{RTR} = \text{rate of temperature rise } [°C\,s^{-1}]$$

$$= (80/60), (1000/3600)°C\,s^{-1}.$$

Table 1. Values of the physical properties and coefficients

| Symbol | Value | Unit |
|---|---|---|
| $a_0$ | $1.1\times10^{-12}$ | m s$^{-1}$ |
| $K_d$ | 1.88 | W m$^{-1}$ K$^{-1}$ |
| $(\rho c_p)_d$ | $1.825\times10^{3}$ | kJ m$^{-3}$ K$^{-1}$ |
| w/c | 0.34 | kg kg$^{-1}$ |
| $\varepsilon$ | 0.16 | |
| $e$ | 0.9 | |
| $\sigma$ | $5.669\times10^{-8}$ | W m$^{-2}$ K$^{-4}$ |
| $D_f$ | 10 800.0 | s |
| $M_w$ | 18.016 | kg kmol$^{-1}$ |
| $M_a$ | 28.952 | kg kmol$^{-1}$ |
| $M_0$ | 0.1025 (RH = 89%) | m$^3$ m$^{-3}$ |
| $R$ | 8.3143 | kJ kmol$^{-1}$ K$^{-1}$ |
| $h_{c,es}$ | 50.0 | W m$^{-2}$ K$^{-1}$ |
| $h_{c,us}$ | 10.0 | W m$^{-1}$ K$^{-1}$ |
| $h_{D,us}$ | $(1.0\times10^{-7}$–$18.84\times10^{-4})$ | kmol m$^{-2}$ s$^{-1}$ |
| $\phi_\infty$ | 0.0118754 | kmol kmol$^{-1}$ |
| $P_{atm}$ | $1.01325\times10^{5}$ | N m$^{-2}$ |
| $T_\infty$ | 298 | K |

(2) $r = r_o$, outer surface

$$-\left(\frac{P_{atm}D'}{RT}\right)\frac{\partial\phi}{\partial r} = h_{D,us}(\phi-\phi_{\infty,us}) \tag{11}$$

$$P = P_{atm} \tag{12}$$

$$-k\frac{\partial T}{\partial r} = h_{us}(T-T_\infty) \tag{13}$$

where

$$h_{us} = h_{c,us}+e\sigma(T_\infty+T)(T_\infty^2+T^2).$$

The initial conditions are

$$\phi(r,0) = \phi_0, \quad P(r,0) = P_{atm}, \quad T(r,0) = T_\infty \tag{14}$$

where $r_i \leqslant r \leqslant r_o$, $r_i = 80.0$ cm and $r_o = 100.0$ cm.

Equations (6)–(14) form a complete mathematical model for the coupled heat and mass transfer in an axisymmetric hollow concrete cylinder subjected to various severe thermal loads at the inner surface and surrounded at the outer surface by normal atmospheric conditions. The physical properties, coefficients and the boundary conditions considered in this study are summarized in Table 1.

## NUMERICAL ANALYSIS

The purpose of this analysis is to develop an efficient numerical procedure for solving the coupled set of basic equations (6)–(14). These partial differential equations can be expressed in a vectorial form; $U_k$, $k = 1,2,3$. $U_1$, $U_2$, and $U_3$ are functions of the space coordinate, $r$, and time, $t$. They represent the mole fraction of water vapor in the gaseous mixture, $\phi$, pore pressure, $P$, and temperature, $T$, respectively.

A fully implicit finite difference scheme incorporating quasi-linearization of the non-linear coefficients and the mixed derivatives is employed. First, the non-linear coefficients, $A_k,\ldots,L_k$, are quasi-linearized by evaluating all these coefficients at time, $t_n$. This is known as 'lagging' the coefficients. Then using a simple iterative updating procedure, these coefficients can be ultimately evaluated at $t_{n+1}$ as required. To do this, the coefficients are first evaluated at the $n$th lagged level and the system is solved for updated values of $U_k$, $k = 1,2,3$, at the $(n+1)$th level. Thus, the coefficients can be updated repeatedly at the current level. This procedure can be repeated iteratively until changes are sufficiently small. In general, ony two or three iterations are used. Second, the time derivations, $\partial U_k/\partial t$, are rewritten using the first-order forward finite difference scheme. The derivatives $\partial U_k/\partial r$ and $\partial^2 U_k/\partial r^2$ are rewritten using the fully implicit central finite difference scheme of first- and second-order accuracy in space respectively at the new time level, $t_{j+1} = t_j+\Delta t$. In quasi-linearization of those mixed derivatives, $(\partial U_k/\partial r)(\partial U_j/\partial r)$ where $k, j = 1,2,3$, a scheme of Newton linearization of coupling terms, is applied to the fully implicit finite difference representations of the mixed derivatives, and is proceeded as follows [14]:

$$\begin{aligned}\left(\frac{\partial U_k}{\partial r}\frac{\partial U_j}{\partial r}\right)_i^{n+1} &\cong \left(\frac{\partial U_j}{\partial r}\right)_i^{n}\left(\frac{\partial U_k}{\partial r}\right)_i^{n+1} \\ &+\left(\frac{\partial U_k}{\partial r}\right)_i^{n}\left(\frac{\partial U_j}{\partial r}\right)_i^{n+1} - \left(\frac{\partial U_k}{\partial r}\frac{\partial U_j}{\partial r}\right)_i^{n} \\ &\cong \frac{1}{(2\Delta r)^2}((-U_{j,i-1}^n+U_{j,i+1}^n)(-U_{k,i-1}^{n+1}+U_{k,i+1}^{n+1}) \\ &+(-U_{k,i-1}^n+U_{k,i+1}^n)(-U_{j,i-1}^{n+1}+U_{j,i+1}^{n+1}) \\ &-(-U_{k,i-1}^n+U_{k,i+1}^n)(-U_{j,i-1}^n+U_{j,i+1}^n)).\end{aligned} \tag{15}$$

Combining the discrete boundary conditions with the set of implicit finite difference equations, after being quasi-linearized, results in a three-by-three block-tridiagonal system of equations in the form $\hat{A}\hat{U} = \hat{R}$, where $\hat{A}$ is a $3(N-2)\times3(N-2)$ sparse unsymmetric matrix, $\hat{U}$ and $\hat{R}$ are $3(N-2)$ vectors with $N$ being the number of nodes in the $r$-direction.

The set of linearized equations has been solved efficiently by MA28, a set of FORTRAN subroutines for solving sparse unsymmetric linear equations using a variant of Gaussian elimination [15].

## RESULTS AND DISCUSSION

The effect of various rates of temperature rise on the inner surface of a concrete hollow cylinder on the pore pressure, temperature, and moisture content distributions at different times, 14.0 and 64.0 min, is shown in Figs. 3–8. The times have been chosen so that the significant effect of surface temperature rises on the magnitudes and locations of the pore pressure peaks can be illustrated. Also, the temperature gradients and moisture content redistributions, as well as the locations of the moving drying fronts under different rates of surface temperature rise, are clearly revealed. Observing from these figures, the higher the rate of the surface temperature rises, the higher the magnitude of the pore pressure peak attained, and the closer the location of pressure peak to the heated

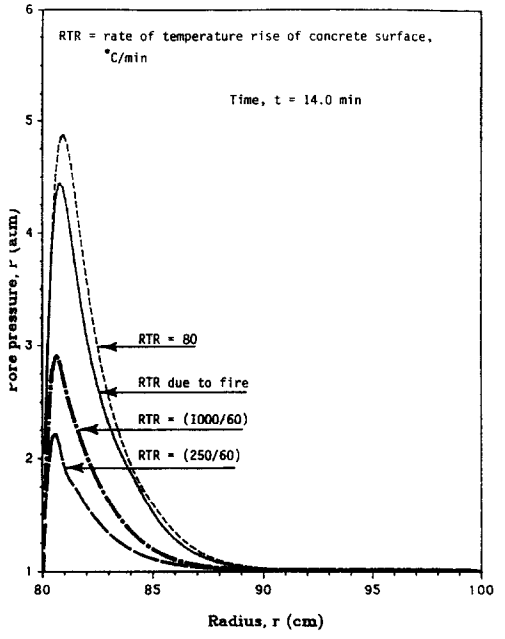


FIG. 3. Effect of heating rate on the pore pressure distributions developed in a hollow concrete cylinder at time of 14.0 min.

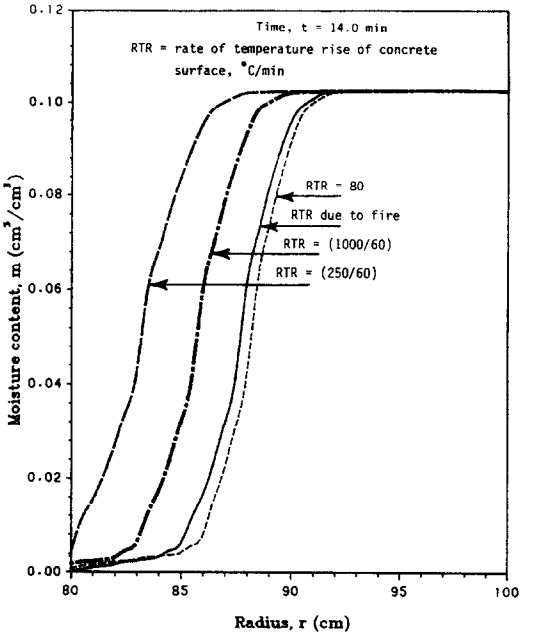


FIG. 5. Effect of heating rate on the moisture content distributions in a hollow concrete cylinder at time of 14.0 min.

inner surface. Also, the locations of the drying front penetrate with time into the concrete cylinder toward the outer surface. The higher the rate of the surface temperature rises, the further is the location of the drying front from the inner surface. Therefore, as one would expect, more moisture loss takes place from the concrete cylinder.

Figures 3–5 exhibit the distributions of the pore pressure, temperature, and moisture content for different heating rates at time 14.0 min. From Fig. 3, for all rates of the surface temperature rise, the pore pressure builds up rapidly beneath the inner surface to reach a maximum value and then subsides as drying continues. Obviously, the higher the rate of the surface

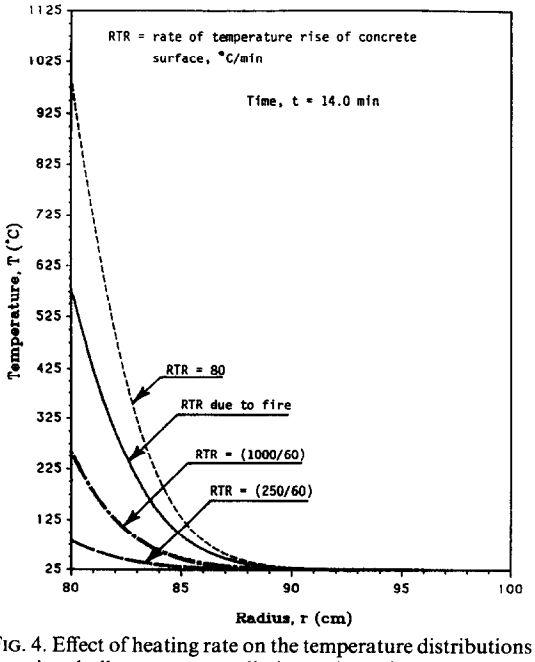


FIG. 4. Effect of heating rate on the temperature distributions in a hollow concrete cylinder at time of 14.0 min.

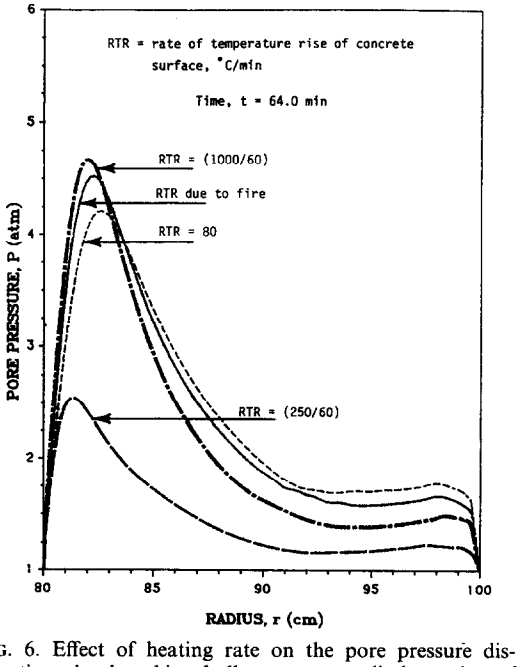


FIG. 6. Effect of heating rate on the pore pressure distributions developed in a hollow concrete cylinder at time of 64.0 min.

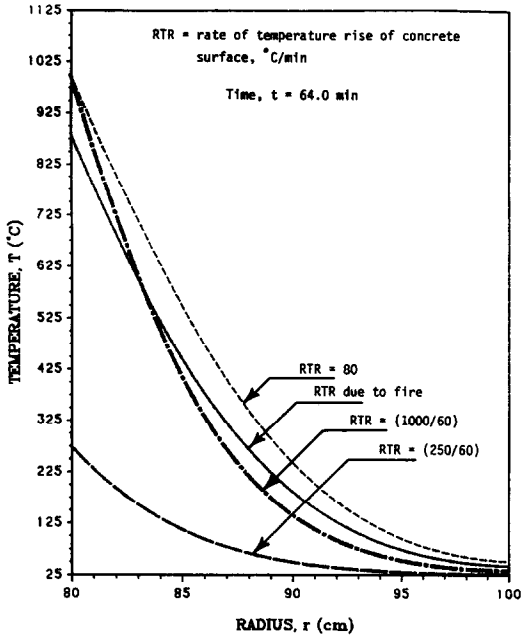


FIG. 7. Effect of heating rate on the temperature distributions in a hollow concrete cylinder at time of 64.0 min.

temperature rises, the larger the magnitude of the pore pressure peak attained. For example, the pore pressure peak developed is approximately 5 atm for the highest rate of surface temperature rise, 80°C $min^{-1}$, and 2.25 atm for the lowest rate, (250/60)°C $min^{-1}$. The higher heat flux entering at the inner surface of the concrete hollow cylinder generates more water vapor in the heated region. The higher pore pressure buildup is caused by the fact that water vapor in the heated region (caused by the higher rate of heat flux) has a narrower passage for escaping than the passage caused by a slower rate of heating. As the drying front penetrates into the concrete cylinder toward the cold surface, $r = r_o$, the pore pressure tends to diminish. That is, as drying proceeds, the moisture content of the concrete cylinder decreases, and, hence, the permeability of concrete increases. As a result, the pore pressure at all locations in the heated region is reduced. Also, a higher rate of surface temperature rise induces a steeper positive pore pressure gradient which indicates a higher rate of decrease in pore pressure and, therefore, a faster rate of drying front penetration moving toward the cold region of concrete. These observations agree with the results of the experimental work carried out by England and Ross [5].

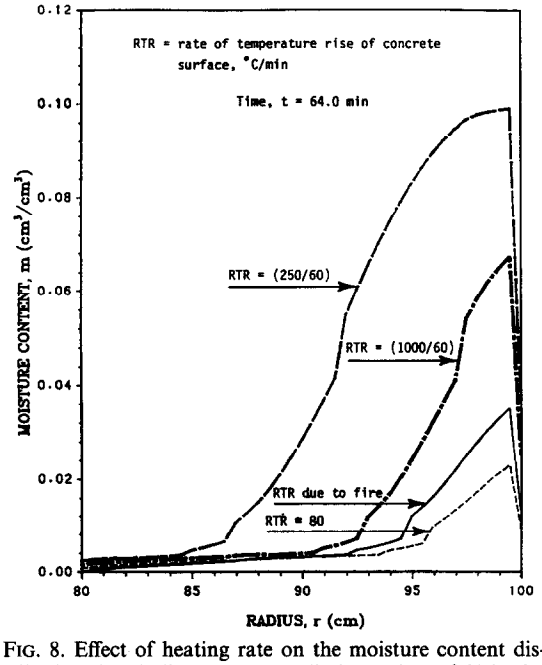


FIG. 8. Effect of heating rate on the moisture content distributions in a hollow concrete cylinder at time of 64.0 min.

Figure 4 illustrates different temperature gradients developed in the heated concrete region (80 cm $\leqslant r \leqslant$ 90 cm), in response to the different rates of the inner surface temperature rise at time 14.0 min. The higher the rate of the surface temperature rise, the steeper is the temperature gradient in the heated zone and the higher is the temperature attained. This agrees with the observed phenomenon of transient conductive heat transfer in concrete.

The comparison of the effect of different rates of surface temperature rise on the moisture content redistributions in the concrete cylinder at time 14.0 min is shown in Fig. 5. Obviously the higher heating rate causes a higher rate of penetration of the moving drying front toward the outer surface. In general, the higher rate of surface temperature rise induces a steeper temperature gradient and higher pore pressure gradient. A higher pore pressure gradient causes a higher range of convective mass flow of gaseous mixture moving toward both the inner and outer surfaces of the concrete cylinder. Therefore, the moving drying front attributed to the higher rate of heating, penetrates deeper into the wall of the concrete cylinder than the slower heating rate does. Many studies show that, when concrete is heated above 100°C, the pore pressure gradient is a dominant mechanism for moisture migration in the high temperature zone, and its effect cannot be neglected [6].

Figures 6–8 show the pore pressure, temperature, and moisture content distributions in a concrete hollow cylinder under the effect of different heating rates of the inner surface at time 64.0 min. Figure 6 shows that the pore pressure peak for the heating rate of (1000/60)°C $min^{-1}$ reaches a maximum value at a radius of 82 cm. At this time, the pore pressure peak for (1000/60)°C $min^{-1}$ grows higher than that for 80°C $min^{-1}$ which attained the maximum pressure peak at time 14.0 min and at 81 cm location (see Fig. 3). This is attributed to the higher moisture content in the peak region of the concrete cylinder for (1000/60)°C $min^{-1}$ at time 64.0 min than the moisture content in the same region for 80°C $min^{-1}$ at this time. From Fig. 7, the temperature gradient at this particular time (64 min) for (1000/60)°C $min^{-1}$ is

steeper than that for 80°C min$^{-1}$. In other words, in the concrete cylinder for the rate at (1000/60)°C min$^{-1}$ has higher heat flux and lower permeability than that for the rate at 80°C min$^{-1}$. Comparison shows that the pore pressure peak for (1000/60)°C min$^{-1}$ is higher than that for (250/60)°C min$^{-1}$ due to the higher surface temperature and the steeper temperature gradient in the concrete cylinder (see Fig. 7). Comparison of Figs. 3 and 6 reveals that the pore pressure peak for the highest heating rate, 80°C min$^{-1}$, is less in value and further outward in location than the peak attained for the same heating rate at time 14.0 min. This reduction in the pore pressure peak between 14.0 and 64.0 min for the rate (1000/60)°C min$^{-1}$ is attributed to the loss of moisture content which in turn results in an increase in the concrete permeability. Also, as time passes, the pore pressure peaks are moving further away from the inner surface. It indicates that the drying front penetrates into the concrete hollow cylinder toward the outer surface as the time advances. In addition, it shows that, for the slowest rate of surface temperature rise, (250/60)°C min$^{-1}$, the pore pressure peak at time 64.0 min is higher than that for 14.0 min. Also, it penetrates into the concrete hollow cylinder toward the outer surface as the time increases. This is an indication that the moisture content around the peak region of the concrete cylinder for (250/60)°C min$^{-1}$ is much higher than that for 80°C min$^{-1}$ in the same region. Therefore, the pore pressure for the lowest heating rate (250/60)°C min$^{-1}$ is continuing to build up and penetrate into the concrete hollow cylinder toward the outer surface with the passage of time.

The corresponding temperature and moisture content distributions for different heating rates at time 64.0 min are shown in Figs. 7 and 8. As one would expect, the rate of the surface temperature rise of (1000/60)°C min$^{-1}$ exhibits the steepest temperature gradient, because at this time the pore pressure peak reaches maximum magnitude for this particular rate (see Fig. 6). However, the fastest rate (80°C min$^{-1}$) has the highest value of temperature distribution.

Figure 8 shows that the higher the rate of the surface temperature rises, the lower the overall moisture content retained in the vessel. Also the location of the moving drying front is moving further away from the inner surface of the concrete cylinder. Notice that the location of the drying front and the location of the pore pressure peak are strongly correlated.

From comparison of temperature gradients due to various heating rates, the effect of the moisture loss on the thermal conductivity can be seen. Moisture loss in concrete decreases its thermal conductivity. This effect impedes the heat transmission through the thickness of the concrete cylinder.

## CONCLUSIONS

The numerical results indicate that the thermal gradient significantly influences the rate of pore pressure buildup and the drying rate in a concrete hollow cylinder exposed to high temperature environments at the inner surface and the surrounding atmosphere at the outer surface. The higher the rate of the concrete surface temperature rise, the higher is the rate of the pore pressure buildup and the higher is the drying rate of the concrete. However, as the drying proceeds to a stage at which all of the concrete cylinder is nearly dry, the effect of the heating rate on the pore pressure and temperature distributions is almost negligible compared to that in the early stage of drying during which the concrete still has much moisture. From these investigations, it is clear that the rate of surface temperature rise significantly influences the maximum value and the location of the pore pressure peak. The higher the rate of surface temperature rise, the higher the rate of pore pressure buildup, and the closer the location of the maximum pore pressure peak to the heated inner surface. Due to the moisture clog and high values of the pore pressure buildup in the clogged region beneath the heated surface of the concrete hollow cylinder, explosive spallings and cracks of the concrete are expected as the stress generated by the pore pressure exceeds the concrete tensile strength.

The results also show that the temperature distributions in the concrete hollow cylinder under different heating rates at the inner surface exhibit the conductive transient phenomenon of heat transfer. Since the loss of moisture in concrete decreases its thermal conductivity, heat transfer from the hot zone to the cold zone is impeded.

In general, the investigation of the effect of the thermal gradient on the pore pressure buildup and drying rate of concrete, qualitatively agree with the results reported elsewhere [7, 10]. Prediction of explosive spallings of concrete due to the moisture clog is of great interest for the fire safety and nuclear reactor safety assessments, as well as for the science and technology of concrete. Also, the numerical results obtained show the influence of the thermal gradients and the moisture contents on the pore pressure developed in concrete. The rate of drying of concrete can be assessed also by the study of heat and mass transfer in porous media, which can be used in the drying technology of concrete products and of masonry.

## REFERENCES

1. T. Z. Harmathy, Moisture and heat transport with particular reference to concrete, National Research of Canada, NRCC 12143, Canada (1971).
2. C. L. D. Huang, H. H. Siang and C. H. Best, Heat and moisture transfer in concrete slabs, *Int. J. Heat Mass Transfer* **22**, 252–266 (1979).
3. C. L. D. Huang, Multi-phase moisture transfer in porous media subject to temperature gradient, *Int. J. Heat Mass Transfer* **22**, 1295–1307 (1979).
4. D. A. Chapman and G. L. England, Effects of moisture migration on shrinkage, pore pressure, and other concrete properties, Trans. 4th Int. Conf. on Structural Mechanics in Reactor Technol., H5/3, pp. 1–14 (1977).

5. G. L. England and A. D. Ross, Shrinkage, moisture, and pore pressures in heated concrete. In *Concrete for Nuclear Reactors*, Vol. 1, American Concrete Institute, Spec. Publ. No. 34, pp. 883–907 (1972).
6. G. O. England and T. J. Sharp, Migration of moisture and pore pressures in heated concrete, 1st Int. Conf. on Structural Mechanics in Reactor Technol., H2/4, pp. 129–143 (1971).
7. G. Dhatt, M. Jacquemier and C. Kadje, Modeling of drying refractory concrete, *Drying 86, Proc. 5th Int. Symp. on Drying*, McGill University, pp. 94–104 (1986).
8. M. S. Sahota and P. J. Pagni, Heat and mass transfer in porous media subject to fires, *Int. J. Heat Mass Transfer* **22**, 1069–1081 (1979).
9. A. Dayan and E. L. Gleukler, Heat and mass transfer within an intensely heated concrete slab, *Int. J. Heat Mass Transfer* **25**, 1461–1467 (1982).
10. Z. P. Bazant and W. Thonguthai, Pore pressure in heated concrete walls—theoretical prediction, *Mag. Concr. Res.* **31**(107), 67–76 (1979).
11. T. Z. Harmathy, Properties of building materials: bases for fire safety design. In *Design of Structures against Fire* (Edited by R. D. Anchor, H. L. Malhotra and J. A. Purkiss), pp. 87–105. Elsevier Applied Science, Amsterdam (1986).
12. U. Schneider, Properties of materials at high temperatures, concrete, Department of Civil Engineering, University of Kassell, Mönchebergstraße 7, D-3500 Kassell, Germany, 2nd Edn (1986).
13. G. N. Ahmed, Modeling of coupled heat and mass transfer in concrete structures exposed to elevated temperatures, Ph.D. Thesis, Kansas State University, Manhattan, Kansas (1990).
14. C. L. D. Huang and G. N. Ahmed, Computational solution for heat and mass transfer in concrete slabs under fire, *Proc. 6th Int. Conf. on Numerical Methods in Thermal Problems*, Swansea, U.K., pp. 960–970 (1989).
15. I. S. Duff, MA28—A set of FORTRAN subroutines for sparse unsymmetric linear equations, Computer Science and Systems Division, AERE Harwell (1980).

## REPONSES DYNAMIQUES DANS DES CYLINDRES CREUX DE BETON SOUS DES CHARGES THERMIQUES ALEATOIRES

**Résumé**—La prédiction de l'intégrité structurelle des réacteurs nucléaires à haute température, sous des environnements thermiques hostiles, est d'un intérêt considérable dans l'estimation de la sécurité des réacteurs. On a établi et résolu numériquement un modèle mathématique qui simule le transfert couplé de chaleur et de masse dans des structures en béton exposées à des températures très élevées. Avec la prédiction de la pression de pore, de la température et de la distribution d'humidité, on étudie l'effet des charges thermiques sur la réponse du béton. Le flux d'humidité pénétrant dans le cylindre et les positions des pics de pression de pore sont déterminés. Ainsi on étudie et prédit les possibilités de feuilletage du béton sous de telles conditions.

## DYNAMISCHE ANTWORT IN BETONHOHLZYLINDERN BEI GEFÄHRLICHER THERMISCHER BEANSPRUCHUNG

**Zusammenfassung**—Die Vorhersage der Strukturstabilität von nuklearen Hochtemperatur-Reaktoren unter ungünstigen thermischen Bedingungen ist ein wichtiger Gesichtspunkt bei der Bewertung der Reaktorsicherheit. Es wird ein mathematisches Modell entwickelt, welches den gekoppelten Wärme- und Stofftransport in Betonstrukturen bei extrem hoher Temperatur beschreibt. Die Lösung erfolgt numerisch. Durch Berechnung des Porendrucks, der Temperatur und der Umverteilung der Feuchtigkeit wird der Einfluß unterschiedlicher thermischer Beanspruchungen auf das Verhalten des Betons untersucht. Bei unterschiedlicher thermischer Belastung wird die Eindringtiefe der Feuchtigkeit in den Betonzylinder und damit der Ort des maximalen Porendrucks bestimmt. Die Möglichkeit der Rißbildung im Beton wird für diese Bedingungen untersucht und vorhergesagt.

## ДИНАМИЧЕСКИЕ ХАРАКТЕРИСТИКИ ПОЛЫХ БЕТОННЫХ ЦИЛИНДРОВ В УСЛОВИЯХ КРИТИЧЕСКИХ ТЕПЛОВЫХ НАГРУЗОК

**Аннотация**—Определение структурной целостности высокотемпературных ядерных реакторов при неблагоприятных тепловых условиях представляет значительный интерес для оценки безопасности реакторов. В данной работе разрабатывается математическая модель, описывающая взаимосвязанный тепло- и массоперенос в бетонных конструкциях, подверженных воздействию экстремальных температур, и находится численное решение этой задачи. На основе расчетов давления, температуры и перераспределения влаги в порах исследуется влияние нестационарных тепловых нагрузок на характеристики бетона. Определяются скорости распространения "закупорки" влаги в бетонном цилиндре, а, следовательно, расположения пиков давления в порах при различных скоростях экстремальных тепловых нагрузок. Таким образом, исследуются возможности растрескивания бетона в рассматриваемых условиях.